Crespo-Bardera, E., Rodríguez, M., Sánchez-Fernández, M., Rajo-Iglesias, E., Feick, R. y Valenzuela, R. A. (2019). Empirical Rates Characterization of Wearable Multi-Antenna Terminals for First-Responders. *IEEE Access*, 7, pp. 6990-7000.

DOI: https://doi.org/10.1109/ACCESS.2019.2890877

IEEE Access
Multidisciplinary | Rapid Review | Open Access Journal

Received December 14, 2018, accepted December 30, 2018, date of publication January 4, 2019, date of current version January 23, 2019.

*Digital Object Identifier 10.1109/ACCESS.2019.2890877*

# Empirical Rates Characterization of Wearable Multi-Antenna Terminals for First-Responders

**ESTEFANÍA CRESPO-BARDERA[1], MAURICIO RODRÍGUEZ[2], (Senior Member, IEEE), MATILDE SÁNCHEZ-FERNÁNDEZ[1], (Senior Member, IEEE), EVA RAJO-IGLESIAS[1], (Senior Member, IEEE), RODOLFO FEICK[3], (Senior Member, IEEE), AND REINALDO A. VALENZUELA[4], (Fellow, IEEE)**

[1]Signal Theory and Communications Department, Universidad Carlos III de Madrid, 28911 Leganés, Spain
[2]Escuela de Ingeniería Eléctrica, Pontificia Universidad Católica de Valparaíso, Valparaíso 2362804, Chile
[3]Department of Electronics Engineering, Universidad Técnica Federico Santa María, Valparaíso 2390123, Chile
[4]Bell Laboratories, Nokia Bell Labs, Holmdel, NJ 07733, USA

Corresponding author: Estefanía Crespo-Bardera (ecrespo@tsc.uc3m.es)

This work was supported in part by the Spanish Government under Project MIMOTEX (TEC2014-61776-EXP), Project CIES (RTC-2015-4213-7), and Project TERESA-ADA (TEC2017-90093-C3-2-R) (MINECO/AEI/FEDER, UE), and in part by the Chilean Government through projects CONICYT under Grant Proyecto Basal FB0821, Grant Fondecyt Iniciación 11171159, and Grant VRIEA-PUCV 039.462/2017.

**ABSTRACT** Empirical characterization of the achievable rates for a wearable multi-antenna terminal shows the potential advantages of deploying a large number of antennas at the user end. We focus on the challenges and requirements of the broadband communication in future emergency communication systems, specifically addressing the outdoor–to–indoor propagation scenario, where the first responder is within an underground area such as a garage or basement. The measurement campaign undertaken characterizes the flat fading multiple-input multiple-output (MIMO) channel matrices at 3.5 GHz for a maximum of $M = 30$ antennas deployed at the base station (BS), and $N = 12$ wearable antennas at the user. The achievable rates are obtained for two transmission strategies that account for the different levels of channel knowledge. In both cases, all the MIMO processing is carried out at the BS.

**INDEX TERMS** Wearables, massive MIMO, textile antenna technology, channel measurements, emergency communications, PMR.

## I. INTRODUCTION

Challenging demands in emergency communications to support first responders and disaster relief activities [1], [2] are overwhelming legacy narrowband Private Mobile Radio (PMR) emergency systems. Up to now, critical communications have mostly been focused to offer a rich set of voice-centric services like group call, direct mode or push-to-talk communications [3]. Nevertheless, following the new trends in wide-band always-on communication systems, a seamless access to novel communication capabilities such as high-resolution images, thermal vision, augmented and/or virtual reality and cognition, video transmission, access remote databases or real-time high-resolution maps would be key in order to solve or alleviate any disaster situation.

4G wireless communication systems such as Long-Term Evolution (LTE) and LTE Advanced-pro propose a portfolio of network capabilities to address emergency specific needs [4], [5]. Two valuable technological approaches within these assets are the exploration of new frequency bands to enlarge the available bandwidth or the deployment of a large number of antennas based on multiple-input multiple-output (MIMO) technology that enables multiplicative capacity gains [2]. Ongoing work for future 5G systems [6], proposes three key frequency ranges to support all the requirements for the next generation of mobile communications including, for example, mobile health care. However, the discussion on which bands should be allocated to future emergency communications is open [7], [8]. Despite the legacy systems still targeting the band below 1 GHz, the clear solution to overcome the current lack of dedicated wide-band spectrum is to allow the coexistence of emergency communication systems with commercial networks (now in the band of $1 - 6$ GHz). Besides this band is going to be gradually refarmed for 5G use. Concretely, the 3.5 GHz Time-Division Long-Term Evolution (TD-LTE) band is being considered as a potential spectrum candidate since it may support higher

data rates due to its larger bandwidth (up to 200 MHz) and it is available in many countries.

MIMO spectral efficiency multiplicative gains are limited unless we also deploy multiple antennas at the user end (UE), facing in this case many challenges with respect to the space for the antennas, the energy consumption and the complexity [9]. One of the design alternatives [10] could be to blend textile antennas around the first responder clothing or protection systems, enhancing the UE connectivity capabilities.

Limited propagation data makes it challenging to predict performance on relevant scenarios. Thus, a complete characterization of the performance of a textile MIMO-based solution in these scenarios is of high relevance. Many efforts have been devoted to characterize MIMO indoor-to-indoor (I2I) and outdoor-to-outdoor (O2O) scenarios [11]–[14]. However, from a first responder perspective, the characterization of outdoor–to-indoor (O2I) underground propagation scenarios such as garages, basements and tunnels is highly relevant since they are typical intervention locations with difficult coverage where MIMO gains could make a difference. Specifically, these locations are highly dependent on the materials and physical structure of the buildings , as well as on the outside environment. In the literature, some authors have characterized other O2I propagation environments and evaluated their impact on MIMO system performance [15]–[17].

In contrast to these studies, our contribution is mainly focused on characterizing unexplored indoor locations where the UE is a few meters below the ground level, modeling in this way a realistic O2I emergency environment where communications cannot be always guaranteed. Furthermore, we propose to integrate a portable, lightweight textile antenna array in the UE equipment enabling the deployment of multiple antennas directly at the user end (e.g., clothing, accessories). In our previous work [18], we analyzed a LTE-based textile massive MIMO proposal with synthetic channel samples, enabling, at least theoretically, an enhanced UE with simulated high symmetric data rates. In this work, we propose to empirically characterize data rate performance in a challenging O2I garage–type propagation scenario where the base station (BS) is placed outdoors at ground level and the first responder UE is placed underground. The main contributions of this work are *i)* the implementation of a measurement campaign at 3.5 GHz in several O2I underground scenarios; *ii)* the statistical characterization of fading in these scenarios, particularly the narrow–band MIMO channel matrix comprising small–scale fading and spatial correlation, key for MIMO achievable rate evaluation; *iii)* the statistical characterization of large–scale fading accounting for the received Signal–to–Noise ratio (SNR); iv) the evaluation and comparison of the system achievable rates based on measured channels with the synthetic rates generated using our proposed statistical models.

The rest of this paper is organized as follows. Section II describes the measurement environment, the channel sounder used for the measurements and the textile array deployed at the UE. Section III provides the statistical characterization of the measured channel. Section IV computes, based on the estimated CDFs of the measured channel, the performance in terms of achievable rates and finally some conclusions are drawn in Section V.

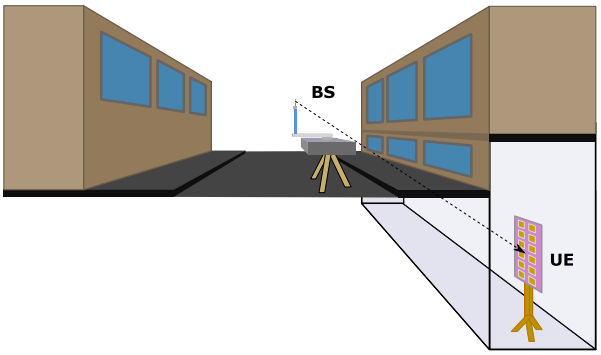


**FIGURE 1.** O2I measurement configuration.

## II. MEASUREMENT LOCATIONS AND EXPERIMENTAL SETUP

### A. MEASUREMENT LOCATIONS

The O2I measurement campaign presented in this work was performed in different scenarios at Universidad Técnica Federico Santa María (UTFSM) in Valparaíso (Chile), using a narrow–band sounding system that operates at 3.5 GHz. In order to ensure the stability of the channel conditions, the measurements were carried out at night without pedestrians or vehicles. It should be noted that despite our use of narrow–band sounding system, our measurements are applicable to broadband communication scenarios since multi–carrier modulations enable a broadband transmission over multiple narrow–band channels.

Trying to emulate the aforementioned emergency O2I environments where conventional communications are not always feasible, the continuous wave 3.5 GHz BS was placed in different outdoor locations on the street next to two different buildings (B1 and B2) selected for the measurement campaign. The UE, consisting of a planar array of textile antennas, was placed indoors underground with respect to the street level (see Fig.1) either in B1 or B2.

The first building (B1) has its floor level 2 m below street level, and the underground room where the UE is placed is 3 m high. The upper portion of the concrete wall facing the street has 1 m high glass windows. There are no doors in the facade that stand between the BS placed outdoor and the UE placed indoor. The second building (B2) is a tall garage with large 15 $m^2$ glass windows facing a street. Floor level is approximately 3 m below street level, and the total height of the room is 7 m. The building is separated of the street by thick 1 m high concrete walls supporting the aforementioned windows. Again there are no doors in the facade that stand between the BS placed outdoor and the UE placed indoor.

The transmitter emulating a base station was placed at two outdoor locations facing B1 and one outdoor location

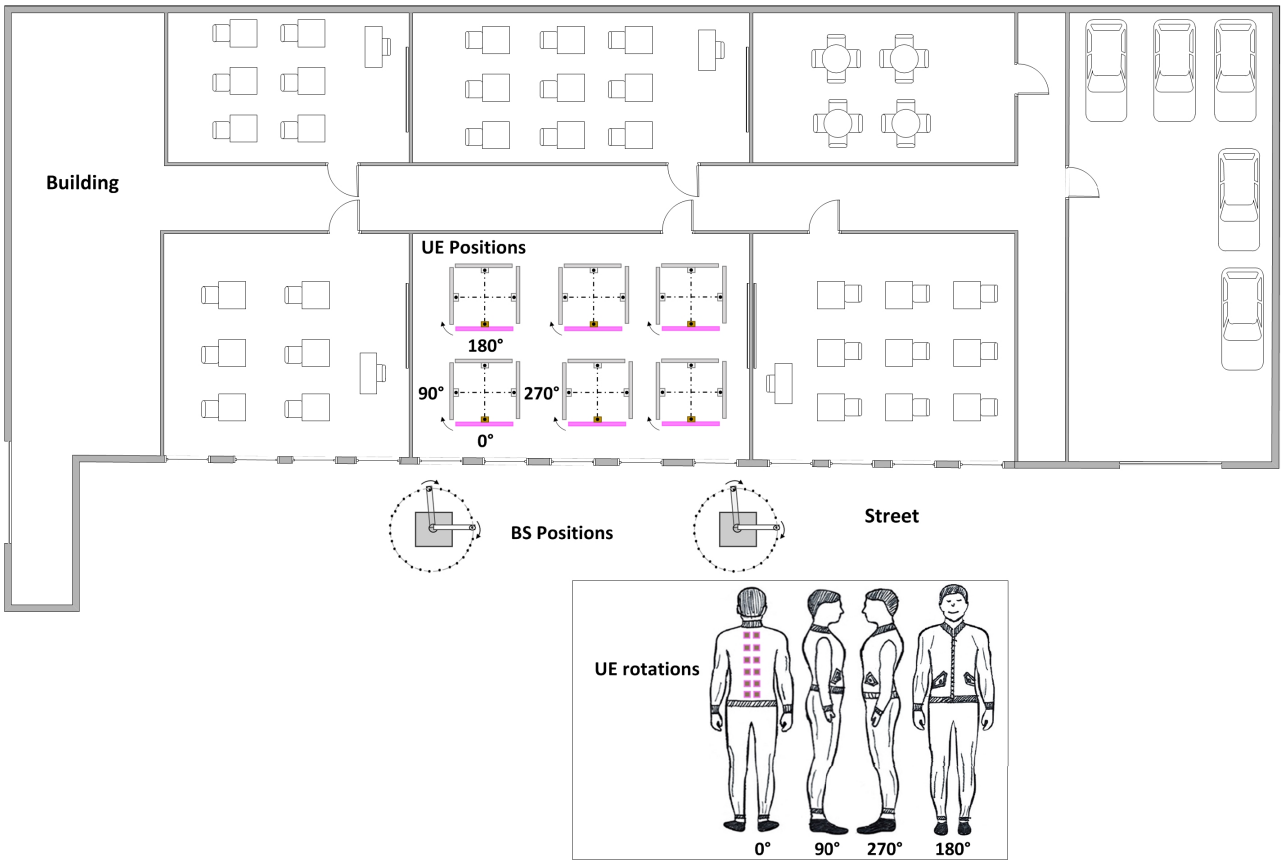


**FIGURE 2.** Measurement location map of Building 1 (B1). Two outdoor positions for the transmitter with the rotating arm and six indoor positions for the UE/first responder, each position with four rotations in 0°, 90°, 180° and 270° with respect to the BS.

facing B2. The measured placements in B1 are shown in Fig. 2 (not drawn to scale). For the two positions of the transmitter, the planar array with the textile antennas was placed in 6 different positions within one underground room. For each indoor location the UE antenna, is oriented in four different angles with respect to the BS (0°, 90°, 180° and 270°, see Fig.2) emulating a scenario where rescuers have the user equipment integrated in their clothing and they are moving. Similarly, in B2 we measure one outdoor position for the BS and 6 indoor positions with the 4 rotations for the UE. Therefore a total of 72 links have been characterized.

### B. EXPERIMENTAL SETUP

The narrow–band MIMO transmitter uses a classic synthetic aperture array [19] where a single element is moved sequentially along the element positions corresponding to the array being synthesize. Specifically, a dipole antenna mounted on a 0.5 m rotating arm (see Fig. 3) and moved in 12° angular increments in the horizontal plane, synthesizing circular array with up to 30 elements. The inter-element distance is $\times 2.8$ the half wavelength ensuring minimal mutual coupling (MC) and thus, correlation at the transmitter will mostly be dependent on the channel scattering characteristics.

At the receiver side, the textile antenna array deployed at the user equipment is composed of individual squared patch antennas of length 3.3 cm using a 0.3 cm thick felt (with permittivity $\epsilon_r = 1.38$) as a dielectric material. Its geometry follows $N_h = 2$ columns in the horizontal plane and $N_v = 6$ antenna rows in the vertical plane. Then, the total array size is $N = N_v \times N_h = 12$ antennas occupying $15 \times 38$ cm$^2$. To minimize MC between antennas at the receiver we selected an inter-element distance of $0.7\lambda$, obtaining simulated MC values below $-20$ dB. The design and characterization of antenna parameters such as MC were performed using CST Microwave Studio. As illustrated in Fig. 3, groups of 4 antennas are connected to 3 SP4T switches, which successively connect one antenna from each group to the input of a 4–channel receiver. The fourth receive channel is used to correct for the phase drift between transmitter and receiver during the measurement sequence. This way for each transmit antenna position, 12 channels to the respective UE antennas are measured.

The channel sounder uses the procedure described in [20] to measure the complex path–gains that form the MIMO channel matrix for each of the $L = 72$ radio links (each corresponding to a different relative position of the transmitter and receiver). The transmitter is continuously transmitting a 14.4 dBm wave carrier at 3.5 GHz. For each of the 30 angular positions of the transmit antenna, the receiver output is sampled at $2 \times 10^5$ samples/s by a data acquisition card for 1 second. This time record is partitioned into

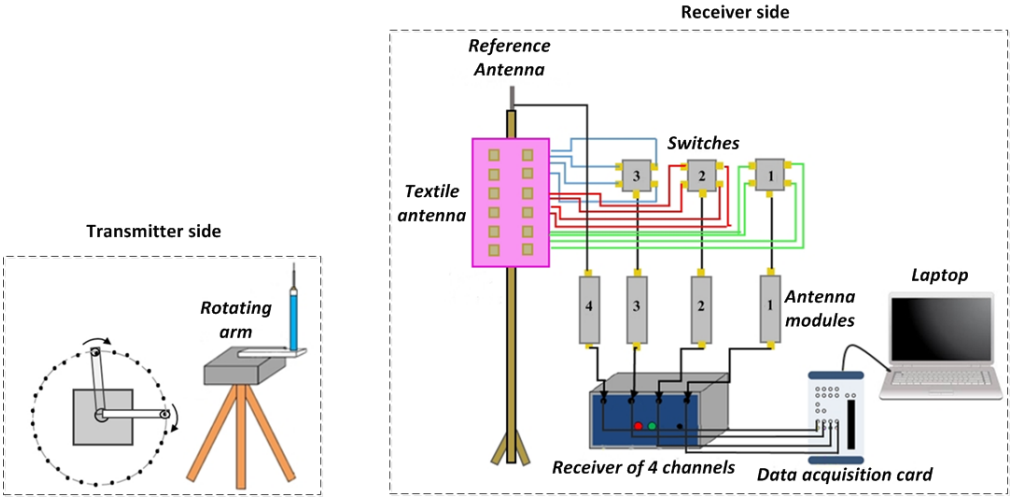


**FIGURE 3.** Channel sounder. Description of the transmitter side with the dipole antenna connected to a rotating arm implementing 30 different positions for the transmit antenna. Description of the receiver side including the textile planar array, the 4–channel receiver module, data acquisition card and processing laptop.

100 subintervals, each of which contains an integer number of cycles of the received sinusoid. To extract the amplitude and phase of the fading coefficient, we apply the Fast Fourier Transform (FFT) to the samples for each subinterval. The fact that for each 1-second acquisition we obtain 100 closely-spaced measurements allows verifying proper equipment operation as our measurement procedure includes verifying that these are consistent. In the case of the amplitude this corresponds to variations of less than 0.5 dB. Averaging these 100 measurements further reduces the measurement noise.

Finally, the relative phase of each channel was obtained as the phase difference with respect to the reference antenna. Transmitter and receiver are locked to GPS disciplined sources which assures phase coherence during the measurement for each group of 3 UE antennas. The phase shift that occurs at the transmitter while sequentially switching between each group of 3 antennas is compensated using the reference channel which continuously tracks this phase.

## III. CHANNEL STATISTICS AND MODELING

The measurement campaign undertaken to characterize the O2I underground scenario, as detailed in Section II provides the relevant information to statistically model our O2I propagation scenarios. In this Section we present the theoretical background for the model–parameter estimation, which includes the choice of estimators and the validation of the model fit. A total of 72 $12 \times 30$ channel matrices were measured and processed to extract all the required parameters. We describe the characterization of small–scale fading, path–loss and spatial fading, providing the basis for the data–rate calculations to be discussed in Section IV.

### A. SMALL-SCALE FADING STATISTICS

Channel small–scale statistics are expected to follow, in most propagation scenarios, a Rayleigh/Ricean distribution. If that is the case, the normalized baseband channel matrices obtained in our measurement campaign should match the following general Ricean model:

$$\mathbf{H} = \sqrt{\frac{K}{K+1}}\mathbf{H}_{\text{LOS}} + \sqrt{\frac{1}{K+1}}\mathbf{H}_{\text{NLOS}} \tag{1}$$

This model characterizes the channel as a combination of both specular and diffuse propagation signal components. The former are represented by the deterministic gain–matrix $\mathbf{H}_{\text{LOS}}$, while the latter are characterized by the matrix $\mathbf{H}_{\text{NLOS}}$, which consists of complex Gaussian elements. $K$ is the Rician $K$–factor, which characterizes the small–scale fade behavior for each of the $N \times M$ propagation channels conforming the $\mathbf{H}$ matrix [21]. We note that while the notation may suggest that for line-of-sight (LOS) scenarios only the first term exists and conversely for non-line-of-sight (NLOS) $\mathbf{H} = \mathbf{H}_{\text{NLOS}}$, actual channels will normally not match such extreme conditions. Specifically, a dominant signal component may exist even in severely obstructed environments, while the LOS condition does not preclude the presence of diffuse multipath propagation. Finally, assuming a separable spatial correlation model [22], $\mathbf{H}_{\text{NLOS}} = \sqrt{\mathbf{R}}\mathbf{H}_{\text{iid}}\sqrt{\mathbf{T}}$ is a $N \times M$ complex Gaussian random matrix with zero mean and $\mathbb{E}\left[\|\mathbf{H}_{\text{NLOS}}\|_F^2\right] = N \times M$ and $\mathbf{T}$ and $\mathbf{R}$ model the spatial correlation at the transmitter and receiver respectively that depend on the antenna deployments and on the scattering characteristic of the channel [23]. $\mathbf{H}_{\text{iid}}$ is an i.i.d. complex Gaussian random matrix that would account for the diffuse propagation with no correlation. Finally, H is normalized by its Frobenius norm as $\|\mathbf{H}\|_F^2 = N \times M$.

Then, under the assumption that the small–scale fading matrix $\mathbf{H}$ can be modeled as in (1), there are 3 parameters, the Rician $K$–factor and the 2 channel correlation matrices that need to be estimated from the measurements. This is going to be done in Sec. III-A.1 and Sec. III-A.2 respectively. With this aim $K$ will be modeled as a position–dependent

random variable, i.e. as a function of the specific characteristics of the place where the terminal is positioned. Given the nature of the test locations of interest, we will be facing the challenging condition of estimating small Ricean $K$–factor values [24]. With regard to the correlation matrices we will make the simplifying assumption that they do not vary significantly with location and that thus one set of values adequately models our environment. As it will be seen, with proper choice of parameters, this simple model adequately describes the achievable spectral efficiency, illustrating its reduction with respect to assuming a strictly Rayleigh channel ($K = 0$).

#### 1) CHARACTERIZATION OF THE RICEAN FACTOR

The measurement campaign described in Section II-A has provided $L = 72$ different channel matrices representing different positions between the transmitter and receiver with $N = 12$ receivers in the textile planar array and a range of transmitters going from $M = 1 \ldots 30$. We assume that $K$–factor is independent of the number of antennas and it does not change unless the surroundings of the transmitter and receiver vary.

The methods available to estimate the $K$–factor based on channel samples depend on the level of information available about the fading coefficients. For single–input single–output (SISO) links, i.e. scenarios with $M = N = 1$, if only the fading coefficients amplitude is available, several approaches explore the relation between different statistical moments of the random envelope to estimate $K$ [25], [26]. If both phase and amplitude are available, more accurate methods exist that can eliminate the bias that affects amplitude-based methods [27], [28]. Similarly, in MIMO links the estimation of the Ricean component can be done using only the amplitude information of the components of the channel matrix applying the SISO philosophy [25], [26]. If the phase information is to be used in MIMO to estimate the $K$–factor, one must first estimate the phase variations of the dominant component resulting from antenna movement of the virtual array from those due to the diffuse components. This has been reported in practice [29] for straight line movement but is very complex for a MIMO geometry with body worn antennas and a circular BS array such as here tested.

Given the difficulty of using phase information with body worn antennas, we use next the amplitude–based estimator $\hat{K}_{\mathrm{A}}$ defined as follows [25]:

$$\hat{K}_{\mathrm{A}} = \frac{\sqrt{1-\gamma}}{1-\sqrt{1-\gamma}} \tag{2}$$

where

$$\gamma = \frac{\mathbb{E}\left[|h|^4 - \mathbb{E}\left[|h|^2\right]^2\right]}{\mathbb{E}\left[|h|^2\right]^2}, \tag{3}$$

$h$ is the complex channel coefficient of a SISO link and $|\cdot|$ is the amplitude.

Based on our data we will illustrate that under the assumption of a channel model described by (1), a single value of the $K$–factor does not properly describe our scenario, so the $K$–factor is going to be be modeled next as an environment–dependent random variable. As a first step we have applied the Kolmogorov-Smirnov goodness–of–fit test (KS test) with a significance level of 0.05 to each of the 72 measured links. The KS test determines that with proper choice of parameters the links' small–scale fading statistics will fit either a Rayleigh or a Rice distribution. This means that there is LOS type small–scale fade behavior with measurable specular component, despite the heavily obstructed nature of the channel at some nominally NLOS locations.

In each position of the transmitter and receiver (link), we obtain an estimation for the $K$-factor using (2) and (3). For each emplacement we have $L_{\mathrm{est}} = 30 \times 12 = 360$ SISO channel measurements, which are used to estimate the averages in (3) allowing a reasonably accurate estimation of the $K$–factor in that position [25]. Indeed, we have found via simulation that for this number of samples $\hat{K}_{\mathrm{A}}$ has a normalized root mean square error (RMSE) of $-2.8$ dB for $K = -3$ dB and $-7.8$ dB for $K = 3$ dB. Also, it is well known that the estimator $\hat{K}_{\mathrm{A}}$ in (2) provides negative non–feasible values for very low–values of $K$. In this scenario, there are two options that have been previously reported in the literature, either to set these values to zero assuming that a low $K$ value was being estimated or to set these values to its absolute value. In the results shown next we will use the latter.

For each of the 72 links we have an estimate for $K$, and from this we obtain the empirical CDF for the $K$–factor as shown it in Fig. 4. The model fit was obtained applying maximum likelihood estimation (MLE) resulting in average $\mu_{\hat{K}_{\mathrm{A}}} = -3.5$ dB and standard deviation $\sigma_{\hat{K}_{\mathrm{A}}} = 3.3$ dB. Applying the KS test with a significance level of 0.05 we have corroborated that our estimated values can be assumed to have a Log-Normal distribution. The Log–Normal distribution of the $K$–factor in other measured environments has been reported before in the literature and used for channel modeling [30], [31]. Finally the CDF shown in Fig. 4 indicates that a significant specular component may be present despite the heavily obstructed nature of the channel.

This statistical characterization of the $K$–factor allows us to classify the measured O2I scenario as a quasi–NLOS scenario, opening up the possibility of comparing in next sections the behavior of the empirical achievable rates with respect to that which would be achieved both in pure NLOS locations and in locations with $K$ distribution following Fig. 4.

#### 2) SPATIAL CORRELATION MODELLING

A separable correlation model [22] for the NLOS channel component $\mathbf{H}_{\mathrm{NLOS}}$ detailed in Sec. III-A, allows the following definitions for both correlation matrices [32]:

$$\mathbf{T} = \frac{1}{N}\mathbb{E}\left[\left(\mathbf{H} - \mathbb{E}\left[\mathbf{H}\right]\right)^{\dagger}\left(\mathbf{H} - \mathbb{E}\left[\mathbf{H}\right]\right)\right] \tag{4}$$

$$\mathbf{R} = \frac{1}{M}\mathbb{E}\left[\left(\mathbf{H} - \mathbb{E}\left[\mathbf{H}\right]\right)\left(\mathbf{H} - \mathbb{E}\left[\mathbf{H}\right]\right)^{\dagger}\right] \tag{5}$$

where $(\cdot)^{\dagger}$ represents the conjugate transpose.

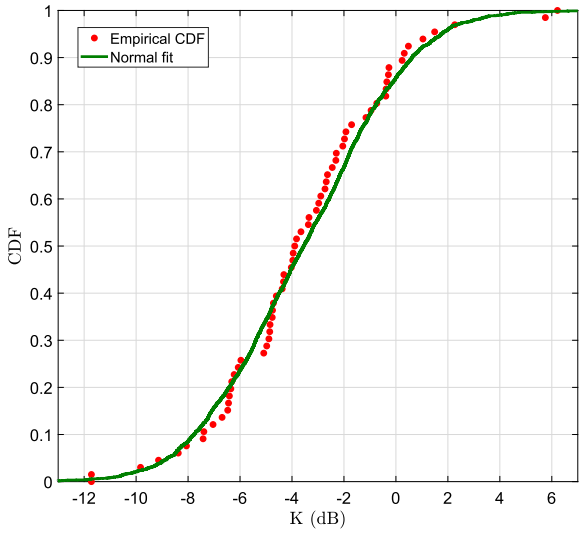


**FIGURE 4.** Estimated CDF for the Ricean factor. A Normal fit for the $\hat{K}$ distribution in dB is provided with parameters $\mu_{\hat{K}_A} = -3.5$ dB and $\sigma_{\hat{K}_A} = 3.3$ dB.

Correlation matrices depend respectively on the antenna characteristics (radiation patterns, mutual coupling, efficiency, etc.), on the antenna geometry (circular array vs planar array) and on the statistical characterization of the power angular spread (PAS) at the transmitter and receiver sides. Considering that all 72 links are geometrically similar, then PAS would not change among the different locations where we place the transmit and receive antennas. Given this, we can estimate both matrices in (4) and (5) from the channel measurements. From these estimated correlation matrices, we provide next a matching to an analytical correlation model for the transmitter and receiver respectively.

The virtual circular array at the transmitter with $M = 30$ should theoretically provide a $M \times M$ symmetric Toeplitz correlation matrix [23], where we can characterize the full matrix if we have the correlation between one of the antenna elements and the other 29 elements (i.e. one of the correlation matrix rows). Furthermore, we have an additional symmetry within the matrix rows, given by the fact that the correlation between one element and the closest 15 elements going through the array clock–wise is the same than moving counter clock–wise. In this scenario, we could fully characterize the channel correlation matrix at the transmitter if we have the correlation between one antenna element and its 15 neighbors in any direction along the circle.

When estimating the channel correlation at the transmitter defined in (4) with the channel measurements, we can easily identify in the obtained correlation matrix the symmetry behavior previously described. Therefore, we proceed to fit correlation coefficients for the 15 antenna elements using the least-squares (LS) method and from there expand to the full correlation matrix. Correlation models proposed in the literature [23] depend on the PAS distribution. Here we test 3 alternatives for the correlation $\mathsf{sinc}(\cdot)$, $\mathsf{exp}(\cdot)$ and rational [23]. Using the least-squares criterion to find the best match we found that the rational function provides the best fit, with an RMSE value of 0.08. For the correlation matrix first row we have $(\mathbf{T})_{1,i} = \frac{b_\mathbf{T}}{a_\mathbf{T}} \frac{a_\mathbf{T}}{(i-1)+b_\mathbf{T}}$ with $i = 1 \ldots 16$ and $(\mathbf{T})_{1,i} = (\mathbf{T})_{1,M+2-i}$ for $i = 17 \ldots 30$ with coefficients $a_\mathbf{T}$ and $b_\mathbf{T}$ as in Table 1. From the $30 \times 30$ correlation matrix, we can also obtain the correlation matrix for different antenna deployments $M < 30$ at the transmitter, simply defining a new Toeplitz matrix truncating the first row $(\mathbf{T})_{1,i}$ to $i = 1 \ldots M$.

**TABLE 1.** Fitting coefficients for spatial correlation matrix modeling at the transmitter T and receiver R.

| $a_\mathbf{T}$ | $b_\mathbf{T}$ | $a_{\mathbf{R}_\theta}$ | $b_{\mathbf{R}_\theta}$ | $a_{\mathbf{R}_\phi}$ | $b_{\mathbf{R}_\phi}$ |
|---|---|---|---|---|---|
| 0.91 | 0.97 | 2.62 | 2.65 | 0.94 | 0.99 |

The correlation at the receiver is a $N \times N$ matrix with $N = 12$ that again, theoretically, could be fully characterized if we model the correlation between one of the antenna elements and the other 11 (i.e. one of the correlation matrix rows). It should be noted that in this case, being the antenna planar array deployed in the vertical plane, correlation is expected to behave differently among antenna elements placed in the same column of the planar array and antenna elements placed in different columns of the planar array. This is so because elevational angle spread has been measured (see [33]) to be much less than the azimuthal spread, therefore antenna elements within the same array column should have a higher correlation than those in different columns of the planar array. When estimating with the channel measurements the channel correlation at the receiver defined by (5), we also observe this behavior. Then, we provide different fits for the antenna elements deployed in the array columns (elevation) and in the array rows (azimuth). Again in both cases different correlation models have been tested ($\mathsf{sinc}(\cdot)$, $\mathsf{exp}(\cdot)$ and rational) and similarly to the transmit scenario the best fit both in azimuth ($\theta$) and in elevation ($\phi$) was obtained using rational functions, however with different parameters. Without loss of generality we number first the antenna elements in the first column of the array followed by the antenna elements placed in the second column. In this scenario, the correlation matrix first row $(\mathbf{R})_{1,i} = \frac{b_{\mathbf{R}_\phi}}{a_{\mathbf{R}_\phi}} \frac{a_{\mathbf{R}_\phi}}{(i-1)+b_{\mathbf{R}_\phi}}$ with $i = 1 \ldots 6$ and $(\mathbf{R})_{1,i} = \frac{b_{\mathbf{R}_\theta}}{a_{\mathbf{R}_\theta}} \frac{a_{\mathbf{R}_\theta}}{(i-N_v)+b_{\mathbf{R}_\theta}}$ with $i = 7 \ldots 12$. The best fit coefficients $a_{\mathbf{R}_\theta}$, $b_{\mathbf{R}_\theta}$, $a_{\mathbf{R}_\phi}$ and $b_{\mathbf{R}_\phi}$ are given in Table 1. It is straightforward to build the correlation matrix with the correlation coefficients of the first row, taking into account the numbering used in the planar array and the relative position between antenna elements.

### B. SPATIAL FADE STATISTICS AND PATH–LOSS

The measurements were carried out for 72 links with distances between the transmitter and receiver ranging from $5 - 11$ m, so the fluctuations in received power are proportional to distance–dependent path–loss (PL) variations and random spatial fade (SF). The variations in received power

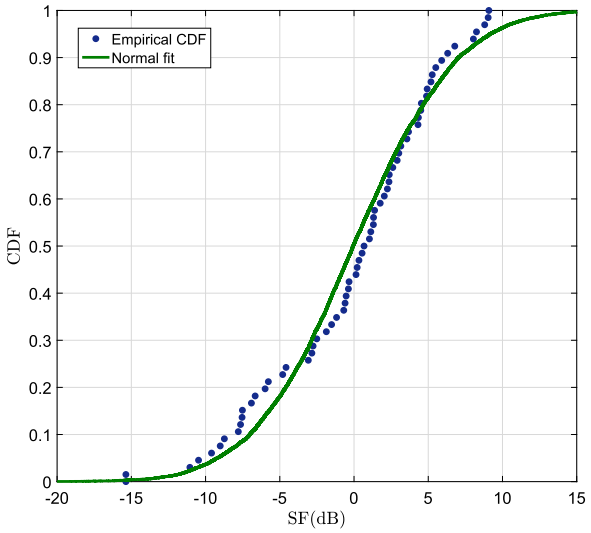


**FIGURE 5.** Measured CDF for normalized shadow fade statistics. The Normal fit for the distribution in dB is provided with parameters $\mu_{SF} \approx 0$, $\sigma_{SF} = 5.5$ dB.

were obtained from the squared Frobenius norm of the measured channel matrices.

Knowing the BS–UE distances, the path–loss exponent is obtained using an LS regression fit of the 72 empirical values of the received power. The PL exponent $\alpha$ is estimated to be 3.32. The free–space excess path–loss is 9.3 dB for a nominal distance of 5 m.

SF values for each link/distance, noted as $P_{\mathrm{SF}}$, are obtained from the received power as the power deviation from the PL computed with path loss exponent $\alpha = 3.32$. Applying KS test with a significance level of 0.05 we verified that the CDF of the empirical values for $P_{\mathrm{SF}}$ matched the classical Log–Normal model [19] very well as shown in Fig. 5. Again, the model fit was obtained applying MLE method. The mean and standard deviation for this model were $\mu_{\mathrm{SF}} \approx 0$ dB and $\sigma_{\mathrm{SF}} = 5.5$ dB respectively. We note that these spatial fades are mostly due to shadow fading as the power variation due to small–scale fades for a $30 \times 12$ random channel matrix is completely negligible when compared to the above results, as is easily confirmed by simulation.

## IV. EMPIRICAL EVALUATION OF THE ACHIEVABLE RATES

The system achievable rates depend on the normalized narrow–band small–scale fading $N \times M$ channel matrix $\mathbf{H}$ (as in (1)) and on the Signal–to–Noise ratio at the receiver, which depends on spatial fades, assuming that distance dependent path–loss is compensated via the BS power control. When precoding at the transmitter is used to overcome spatial interference, the achievable rate (in bits/s/Hz), for Gaussian input signal is given by [34]:

$$R = \log\det\left(\mathbf{I}_N + \frac{\mathsf{SNR}}{\mathrm{Tr}\{\mathbf{Q}\}}\mathbf{H}\mathbf{Q}\mathbf{H}^{\dagger}\right), \tag{6}$$

where SNR denotes the received Signal-to-Noise ratio, $\mathbf{I}_N$ is the $N \times N$ identity matrix, $\mathbf{Q}$ denotes the input covariance matrix chosen depending on the implemented precoding strategy and $\mathrm{Tr}\{\cdot\}$ is the trace operation.

In this work we address two different transmission strategies, each of them characterized by different level of channel information (CSI) at the transmitter:

- *Optimal precoder with CSI at the transmitter (CSIT)*: the transmitter needs to accurately track the instantaneous CSI ($\mathbf{H}$), which may be feasible with the system working in Time Division Duplexing (TDD). It requires a matrix decomposition computation for every channel use since the precoder would instantaneously diagonalize the channel matrix and its squared singular values are given by the optimal water-filling (WF) power allocation [35]. Then $\mathbf{Q} = \mathbf{U}\Lambda\mathbf{U}^{\dagger}$, where $\mathbf{U}$ are the eigenvectors of $\mathbf{H}^{\dagger}\mathbf{H}$, and $\Lambda$ is obtained from the classical WF power allocation algorithm.
- *Optimal precoder with no CSI at the transmitter (No–CSIT)*: the precoder does not perform any processing since it does not have any information about the channel, in which case $\mathbf{Q}$ is set equal to the identity matrix.

In this section we evaluate the achievable rates $R$ of a typical emergency O2I scenario where a first responder equipped with the wearable multi-antenna terminal is positioned indoors in an underground location. The performance of CSIT and No–CSIT is studied based on (6) using the measured channel matrices. This is compared with the results obtained with the simulation model (1) using parameters estimated from our data as described in Section III. The standard procedure of normalization of gain matrices by the Frobenius norm [36] was used to allow setting a SNR that is not affected by scale factors in the measurements or in the simulation. We define for our comparison $\mathsf{SNR}_{\mathrm{ref}}$ as the average value of SNR in a region subject to random (zero–mean) shadow fading, i.e. the value after eliminating shadow fade variations. In the case of the empirical data the distance–dependent path loss is removed using the linear regression discussed in Section III-B. This assumes that transmit power control compensates for large–scale path–loss variation due to changes in distance between base and user, but not for per–instantiation SNR variations due to shadowing.

For the simulation model 3000 complex Gaussian matrices were generated to simulate the diffuse components and in the case of the Rician model, the specular component was generated as an all–ones deterministic matrix [37]. The spatial correlation matrices for the channel synthetic data correspond to the models described in Sec. III-A.2. The shadow fades follow the Log–Normal fitted model described in Sec. III-B, therefore also for the synthetic data, SNR accounts for random shadow fading with $\mathsf{SNR}_{\mathrm{ref}}$ as its average value. For reference we also plot the results for simulated Rayleigh i.i.d. matrices.

We present the achievable rates for different antenna deployments at the transmitter $M = \{2, 4, 12, 30\}$ and

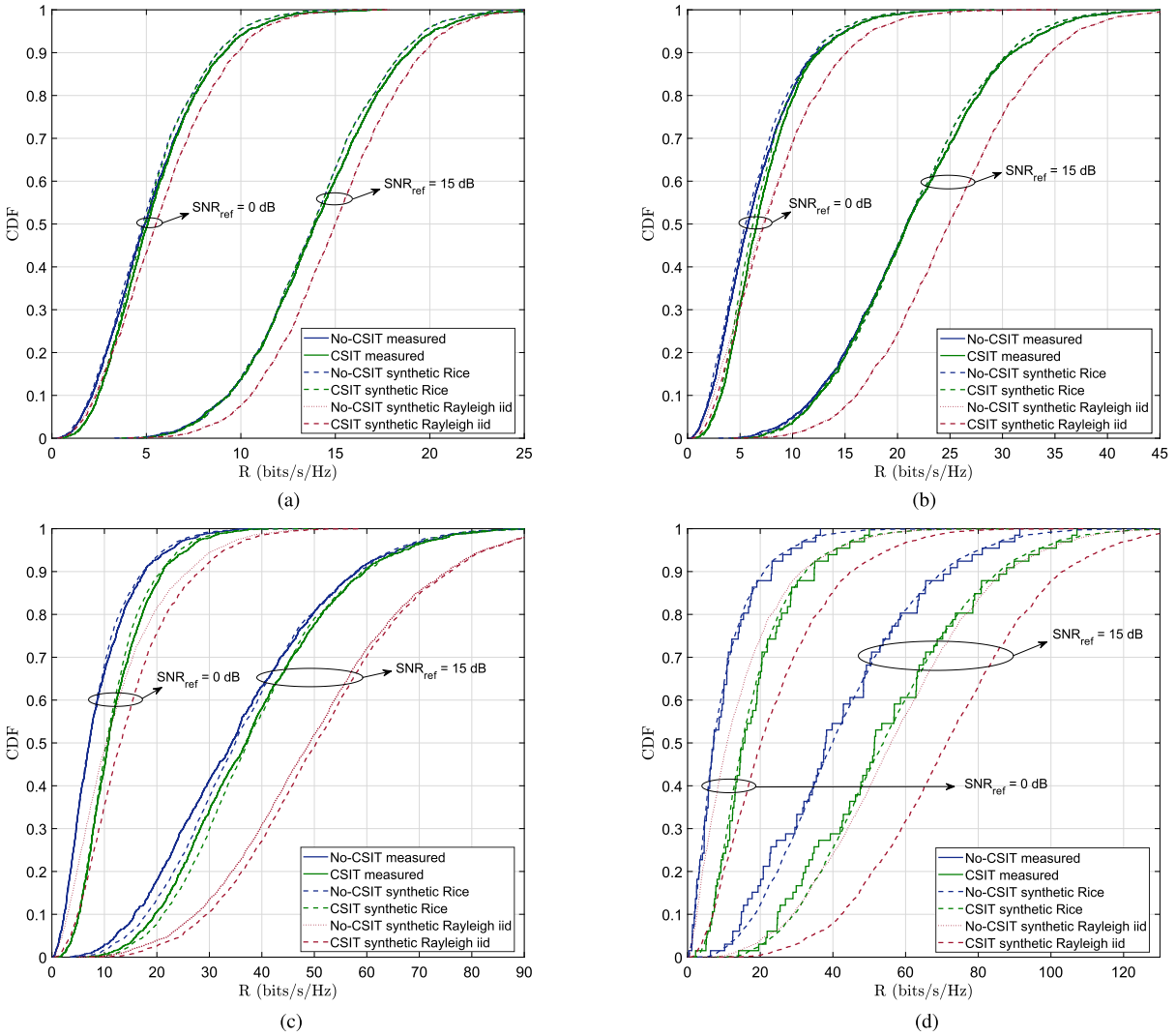


**FIGURE 6.** Achievable rates obtained from the measurement campaign and comparison with Rayleigh iid and correlated Rice channel samples synthetically generated. Different antenna deployments are studied in the BS $M = \{2, 4, 12, 30\}$ and an array of $N = 12$ textile antennas is placed at the user end. (a) Empirical and synthetic $R$ for $M = 2$, $N = 12$ and $\mathrm{SNR}_{\mathrm{ref}}(\mathrm{dB}) = \{0, 15\}$; (b) Empirical and synthetic $R$ for $M = 4$, $N = 12$ and $\mathrm{SNR}_{\mathrm{ref}}(\mathrm{dB}) = \{0, 15\}$; (c) Empirical and synthetic $R$ for $M = 12$, $N = 12$ and $\mathrm{SNR}_{\mathrm{ref}}(\mathrm{dB}) = \{0, 15\}$; (d) Empirical and synthetic $R$ for $M = 30$, $N = 12$ and $\mathrm{SNR}_{\mathrm{ref}}(\mathrm{dB}) = \{0, 15\}$.

$\mathrm{SNR}_{\mathrm{ref}}(\mathrm{dB}) = \{0, 15\}$. The first two scenarios $M = \{2, 4\}$ corresponds to realistic current emergency scenarios, where the BS are still equipped with small number of antennas. The large antenna deployments $M = \{12, 30\}$ accounts for more futuristic 5G scenarios, where much higher rates may be achieved enabling novel communication capabilities such as, high-resolution images, thermal vision, augmented and/or virtual reality and cognition, all candidates for future emergency systems.

Figure 6 shows that using the enhanced multi–antenna UE in the tested O2I emergency scenarios, at high SNR, we can achieve significant increases in data rates. As expected, as the number of antennas increases the spectral efficiency also increases, confirming the expected MIMO gains. Similarly, for high SNR and large number of antennas ($M = \{4, 12, 30\}$) we observe how CSIT outperforms the scenarios where CSI is not available at the transmitter.

Also, the rates obtained from these synthetic channel realizations are seen to match the empirical results very well (see Fig. 6). The predicted spectral efficiencies for the Rayleigh model are as expected the highest, illustrating that even in this heavily obstructed scenario such a model is overly optimistic.

### A. PERFORMANCE WITH DIFFERENT BS CONFIGURATIONS

Since MIMO gains strongly depend on the lowest number of transmit or receive antennas, we evaluate the impact of incrementing the number of antennas at the BS when the number of antennas at the first–responder terminal is fixed to $N = 12$.

In Fig. 7 we provide the achievable rates averaged on the channel realizations for the measured channel data and for two different correlation scenarios of the Ricean synthetic data, one following the correlation models in Sec. III-A.2 and

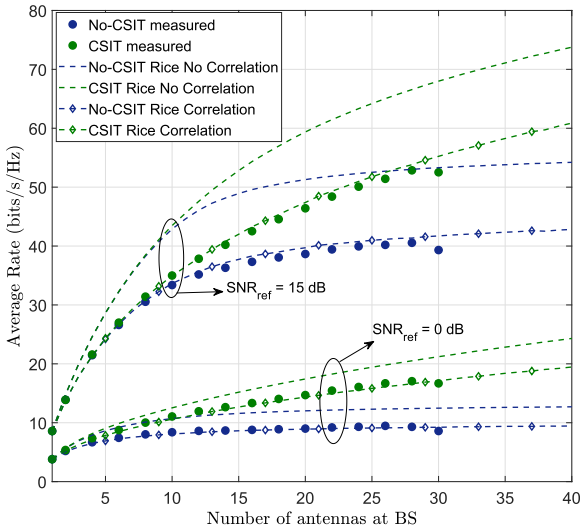


**FIGURE 7.** Comparison of average rates between the measured channel coefficients and synthetic Ricean when increasing the number of antennas at the BS with $\mathsf{SNR}_{\mathbf{ref}}\mathbf{(dB)} = \{0, 15\}$. Synthetic coefficients are generated without and with correlation (empty diamond marker).

the second forcing no correlation, i.e. $\mathbf{T} = \mathbf{I}_M$ and $\mathbf{R} = \mathbf{I}_N$. Fig. 7 clearly shows the saturation effect with almost no additional rate gains for $M$ greater than 20. This behaviour can be explained by the fact that the measured channel matrices are not Gaussian i.i.d. It is well–known [38], that both spatial correlation and Ricean distributions significantly limit the linear growth in spatial multiplexing gain.

The average rates presented for synthetic data, both with the measured correlation matrices and forcing the samples to be uncorrelated, show the relevance of correlation in MIMO performance [38]. It is well–known that for the transmission strategies that we are considering in this work (CSIT and No–CSIT), when the channel is uncorrelated, both transmission strategies perform significantly better than when we have correlation. So this correlation must be inlcuded in the generation of synthetic channel samples for an accurate match to the measured rates.

### B. ENABLING NOVEL COMMUNICATION CAPABILITIES FOR EMERGENCY SCENARIOS

The enhanced multi-antenna terminal solution is proposed as a technology that provides first responders with high throughput capabilities to alleviate, resolve or overcome emergency situations using vital augmented information. Indeed, given that there are already specific throughput requirements for the deployment of broadband services needed in emergency situations [39], we show in Table 2 the throughput achieved in 90% of the measured locations with the enhanced UE terminal and different antenna configurations in the BS. Also, the set of services that would be feasible in our O2I scenario according to [39] are included.

The throughput in Mbps achieved at 90% of the measured locations is obtained as $R_{90\%} \times B$ where $R_{90\%}$ is the rate meeting $P\left(R_{90\%} \leq R\right) = 0.1$ when using the measured channel matrices for No–CSIT and $\mathsf{SNR}_{\mathrm{ref}} = 15$ dB, $B$ represents the available bandwidth that in Table 2 is fixed to 10 MHz.

**TABLE 2.** Provided multimedia services using the enhanced multi-antenna terminal and a bandwidth of 10 MHz and No–CSIT.

| Antenna configuration $N \times M$ | Empirical throughput (Mbps) | Provided Multimedia Services in the O2I scenario |
|---|---|---|
| $12 \times 2$ | 89 | Remote controlling<br>First Responder connectivity |
| $12 \times 4$ | 122 | Video streaming |
| $12 \times 12$ | 169 | E-Health<br>Multi–person video call |

## V. CONCLUSION

We evaluated using measured channels the achievable rates in typical O2I emergency scenarios when the first responder has a multi-antenna terminal for different levels of channel knowledge at the transmitter (CSIT and No–CSIT). Additionally, we have compared these rates with the ones achieved with synthetic channel samples that follow typical measured statistics such as Rayleigh or Rice. Our work demonstrates that the achieved rates are consistently lower than those obtained under the correlated Rayleigh and the Rayleigh i.i.d. assumptions, despite the fact this is a heavily obstructed NLOS scenario. In spite of these conclusions directly related with characteristics of the particular O2I propagation scenario, it is clear that the textile antenna array significantly improves spectral efficiency. Finally, as a future work it will be interesting to carry out other O2I studies applicable to wideband emergency communication requirements for different sets of scenarios and distances and particularly for different frequency bands. Specifically, the comparison of the mmWave option vs lower frequencies such as considered here is a highly relevant topic. This implies studying the tradeoff between high path–losses (i.e. low SNR and lower coverage) at mmWave frequencies in relation to the multi-antenna methods required to achieve adequate data rates within a limited bandwidth.

## REFERENCES

[1] G. Baldini, S. Karanasios, D. Allen, and F. Vergari, "Survey of wireless communication technologies for public safety," *IEEE Commun. Surveys Tuts.*, vol. 16, pp. 619–641, 2nd Quart., 2014.
[2] M. Mezzavilla *et al.*, "Public safety communications above 6 GHz: Challenges and opportunities," *IEEE Access*, vol. 6, pp. 316–329, 2017.
[3] A. Kumbhar, F. Koohifar, I. Güvenç, and B. Mueller, "A survey on legacy and emerging technologies for public safety communications," *IEEE Commun. Surveys Tuts.*, vol. 19, no. 1, pp. 97–124, 1st Quart., 2017.
[4] T. Doumi *et al.*, "LTE for public safety networks," *IEEE Commun. Mag.*, vol. 51, no. 2, pp. 106–112, Feb. 2013.
[5] R. Ferrus and O. Sallent, "Extending the LTE/LTE-A business case: Mission- and business-critical mobile broadband communications," *IEEE Veh. Technol. Mag.*, vol. 9, no. 3, pp. 47–55, Sep. 2014.

[6] *5G Spectrum Public Policy Position*, GSM Assoc., London, U.K., 2016.

[7] M. M. Sohul, M. Yao, X. Ma, E. Y. Imana, V. Marojevic, and J. H. Reed, "Next generation public safety networks: A spectrum sharing approach," *IEEE Commun. Mag.*, vol. 54, no. 3, pp. 30–36, Mar. 2016.

[8] R. Fantacci, F. Gei, D. Marabissi, and L. Micciullo, "Public safety networks evolution toward broadband: Sharing infrastructures and spectrum with commercial systems," *IEEE Commun. Mag.*, vol. 54, no. 4, pp. 24–30, Apr. 2016.

[9] F. Rusek *et al.*, "Scaling up MIMO: Opportunities and challenges with very large arrays," *IEEE Signal Process. Mag.*, vol. 30, no. 1, pp. 40–60, Jan. 2013.

[10] M. Sánchez-Fernández, A. Tulino, E. Rajo-Iglesias, J. Llorca, and A. G. Armada, "Blended antenna wearables for an unconstrained mobile experience," *IEEE Commun. Mag.*, vol. 55, no. 4, pp. 160–168, Apr. 2017.

[11] J. W. Wallace, W. Ahmad, Y. Yang, R. Mehmood, and M. A. Jensen, "A comparison of indoor MIMO measurements and ray-tracing at 24 and 2.55 GHz," *IEEE Trans. Antennas Propag.*, vol. 65, no. 12, pp. 6656–6668, Dec. 2017.

[12] J. W. Wallace, M. A. Jensen, A. L. Swindlehurst, and B. D. Jeffs, "Experimental characterization of the MIMO wireless channel: Data acquisition and analysis," *IEEE Trans. Wireless Commun.*, vol. 2, no. 2, pp. 335–343, Mar. 2003.

[13] D. Chizhik, J. Ling, P. W. Wolniansky, R. A. Valenzuela, N. E. Costa, and K. Huber, "Multiple-input-multiple-output measurements and modeling in Manhattan," *IEEE J. Sel. Areas Commun.*, vol. 21, no. 3, pp. 321–331, Apr. 2003.

[14] R. Zhang, X. Lu, J. Zhao, L. Cai, and J. Wang, "Measurement and modeling of angular spreads of three-dimensional urban street radio channels," *IEEE Trans. Veh. Technol.*, vol. 66, no. 5, pp. 3555–3570, May 2017.

[15] V. Kristem *et al.*, "3D MIMO outdoor-to-indoor propagation channel measurement," *IEEE Trans. Wireless Commun.*, vol. 16, no. 7, pp. 4600–4613, Jul. 2017.

[16] S. Wyne, A. Molisch, P. Almers, G. Eriksson, J. Karedal, and F. Tufvesson, "Outdoor-to-indoor office MIMO measurements and analysis at 5.2 GHz," *IEEE Trans. Veh. Technol.*, vol. 57, no. 3, pp. 1374–1386, May 2008.

[17] Q. Zheng, J. Zhang, H. Yu, Y. Zhang, and L. Tian, "Propagation statistic characteristic of 3D MIMO channel in outdoor-to-indoor scenario with different antenna heights," in *Proc. IEEE 19th Int. Symp. Wireless Pers. Multimedia Commun. (WPMC)*, Nov. 2016, pp. 411–416.

[18] E. Crespo-Bardera, M. Sánchez-Fernández, A. Garcia-Armada, A. G. Martin, and A. F. Duran, "Analysis of a LTE-based textile massive MIMO proposal for public safety networks," in *Proc. IEEE 86th Veh. Technol. Conf. (VTC-Fall)*, Sep. 2017, pp. 1–5.

[19] M. Rodríguez, R. Feick, R. A. Valenzuela, and D. Chizhik, "Achieving near maximum ratio combining diversity gains with directive antennas," *IEEE Trans. Veh. Technol.*, vol. 66, no. 9, pp. 7782–7796, Sep. 2017.

[20] F. Silva, R. Feick, R. A. Valenzuela, M. S. Derpich, and L. Ahumada, "Measurement-based evaluation of spectral efficiencies in outdoor-indoor multiuser MISO systems in femto-cells," *IEEE Trans. Wireless Commun.*, vol. 15, no. 9, pp. 5889–5903, Sep. 2016.

[21] F. R. Farrokhi, G. J. Foschini, A. Lozano, and R. A. Valenzuela, "Link-optimal space-time processing with multiple transmit and receive antennas," *IEEE Commun. Lett.*, vol. 5, no. 3, pp. 85–87, Mar. 2001.

[22] K. I. Pedersen, P. E. Mogensen, and B. H. Fleury, "A stochastic model of the temporal and azimuthal dispersion seen at the base station in outdoor propagation environments," *IEEE Trans. Veh. Technol.*, vol. 49, no. 2, pp. 437–447, Mar. 2000.

[23] M. Sánchez-Fernández, S. Zazo, and R. Valenzuela, "Simplifying the beamforming optimality region for practical MIMO scenarios," *IEEE Commun. Lett.*, vol. 10, no. 11, pp. 751–753, Nov. 2006.

[24] C. M. J. Wang *et al.*, "Parameter estimation and uncertainty evaluation in a low Rician K-factor reverberation-chamber environment," *IEEE Trans. Electromagn. Compat.*, vol. 56, no. 5, pp. 1002–1012, Oct. 2014.

[25] L. J. Greenstein, D. G. Michelson, and V. Erceg, "Moment-method estimation of the Rician $K$-factor," *IEEE Commun. Lett.*, vol. 3, no. 6, pp. 175–176, Jun. 1999.

[26] A. Abdi, C. Tepedelenlioglu, M. Kaveh, and G. Giannakis, "On the estimation of the K parameter for the Rice fading distribution," *IEEE Commun. Lett.*, vol. 5, no. 3, pp. 92–94, Mar. 2001.

[27] Y. Chen and N. C. Beaulieu, "Maximum likelihood estimation of the $K$ factor in Ricean fading channels," *IEEE Commun. Lett.*, vol. 9, no. 12, pp. 1040–1042, Dec. 2005.

[28] K. E. Baddour and T. J. Willink, "Improved estimation of the ricean $K$-factor from I/Q fading channel samples," *IEEE Trans. Wireless Commun.*, vol. 7, no. 12, pp. 5051–5057, Dec. 2008.

[29] T. J. Willink and G. W. K. Colman, "Measurement-based analysis of cross-layer adaptation for mimo in mobile urban environments," *IET Commun.*, vol. 7, pp. 697–705, May 2013.

[30] Y. Hikiyama, H. Tsutsui, and Y. Miyanaga, "MIMO propagation scenario discrimination for adaptive wireless communication systems," in *Proc. 13th Int. Symp. Commun. Inf. Technol. (ISCIT)*, Sep. 2013, pp. 674–679.

[31] S. Zhu *et al.*, "Probability distribution of Rician $K$-factor in urban, suburban and rural areas using real-world captured data," *IEEE Trans. Antennas Propag.*, vol. 62, no. 7, pp. 3835–3839, Jul. 2014.

[32] M. Sánchez-Fernández, S. Zazo, and R. Valenzuela, "Performance comparison between beamforming and spatial multiplexing for the downlink in wireless cellular systems," *IEEE Trans. Wireless Commun.*, vol. 6, no. 7, pp. 2427–2431, Jul. 2007.

[33] H. Xu *et al.*, "MIMO channel capacity for fixed wireless: Measurements and models," in *Proc. IEEE 54th Veh. Technol. Conf. VTC Fall*, vol. 2, Oct. 2001, pp. 1068–1072.

[34] A. Goldsmith, S. A. Jafar, N. Jindal, and S. Vishwanath, "Capacity limits of MIMO channels," *IEEE J. Sel. Areas Commun.*, vol. 21, no. 5, pp. 684–702, Jun. 2003.

[35] H. Huang, C. Papadias, and S. B. Venkatesan, *MIMO Communication for Cellular Networks*. New York, NY, USA: Springer, 2012.

[36] S. Loyka and G. Levin, "On physically-based normalization of MIMO channel matrices," *IEEE Trans. Wireless Commun.*, vol. 8, no. 3, pp. 1107–1112, Mar. 2009.

[37] R. U. Nabar, H. Bolcskei, and A. J. Paulraj, "Diversity and outage performance in space-time block coded Ricean MIMO channels," *IEEE Trans. Wireless Commun.*, vol. 4, no. 5, pp. 2519–2532, Sep. 2005.

[38] A. M. Tulino, A. Lozano, and S. Verdú, "Impact of antenna correlation on the capacity of multiantenna channels," *IEEE Trans. Inf. Theory*, vol. 51, no. 7, pp. 2491–2509, Jul. 2005.

[39] *Communication from the Commission to the European Parliament, the Council, the European Economic and Social Committee and the Committee of the Regions. Connectivity for a Competitive Digital Single Market—Towards a European Gigabit Society*, Eur. Commission, Brussels, Belgium, 2016.


**ESTEFANÍA CRESPO-BARDERA** received the bachelor's degree in communication system engineering, and the master's degree in multimedia and communications from the Universidad Carlos III de Madrid, in 2014 and 2016, respectively. Since 2016, she has been a student of the Multimedia and Communication Inter-University Ph.D. Program from the Universidad Carlos III de Madrid. At the same time, she has been working in public R&D projects, including CIES (RTC-2015-4213-7) and MIMOTEX (TEC2014-61776-EXP), supported by the Spanish Government. She has also performed several research stays at the Universidad Técnica Federico Santa María, Valparaíso, Chile, in 2016, and the University of California at Berkeley, Berkeley, CA, USA, in 2017. Her main research interests include MIMO technology, antenna design, and RF channel modeling for wireless communications.

**MAURICIO RODRÍGUEZ** (S'15-M'17-SM'18) received the degree in Ingeniero Civil Electrónico, and the M.Sc. degree in electronics engineering from the Universidad Técnica Federico Santa María, Valparaíso, Chile, in 2011, and the Ph.D. degree in electronics engineering from the Universidad Técnica Federico Santa María, in 2017. Since 2016, he has been with the Escuela de Ingeniería Eléctrica, Pontificia Universidad Católica de Valparaíso, Valparaíso. His main research interests include RF channel modeling, RF measurement, and microwave system design.

**MATILDE SÁNCHEZ-FERNÁNDEZ** (SM'14) received the M.Sc. degree in telecommunications engineering, and the Ph.D. degree from the Universidad Politécnica de Madrid, Madrid, Spain, in 1996 and 2001, respectively. She was a Telecommunication Engineer with Telefónica. In 2000, she joined the Universidad Carlos III de Madrid, Madrid, where she has been an Associate Professor, since 2009, teaching several undergraduate and graduate courses (M.Sc. and Ph.D.), related to communication theory and digital communications. She performed several research stays at the Information and Telecommunication Technology Center, The University of Kansas, Lawrence (1998), Bell Laboratories, Crawford Hill, NJ, USA (2003–2006, 2015), Centre Tecnològic de Telecomunicacions de Catalunya, Barcelona, Spain (2007), and Princeton University, Princeton, NJ, USA (2011). Her current research interests are signal processing for wireless communications, multiple-input multiple-output techniques, channel modeling in wireless communications, and game theory and machine learning techniques applied to communications. In these fields, she has co-authored over 50 contributions to international journals and conferences.

**EVA RAJO-IGLESIAS** (SM'08) was born in Monforte de Lemos, Spain, in 1972. She received the M.Sc. degree in telecommunication engineering from the University of Vigo, Vigo, Spain, in 1996, and the Ph.D. degree in telecommunication engineering from the University Carlos III of Madrid, Madrid, Spain, in 2002. She was a Teaching Assistant with the University Carlos III of Madrid, from 1997 to 2001. She joined the Polytechnic University of Cartagena, Cartagena, Spain, as a Teaching Assistant, in 2001. She joined the University Carlos III of Madrid, as a Visiting Lecturer, in 2002, where she has been an Associate Professor with the Department of Signal Theory and Communications, since 2004. She visited the Chalmers University of Technology, Gothenburg, Sweden, as a Guest Researcher, from 2004 to 2008, where she has been an Affiliate Professor with the Antenna Group, Signals and Systems Department, since 2009. She has co-authored over 50 papers in JCR international journals, and more than 100 papers in international conferences. Her current research interests include microstrip patch antennas and arrays, metamaterials, artificial surfaces and periodic structures, gap waveguide technology, MIMO systems, and optimization methods applied to electromagnetism. She was a recipient of the Loughborough Antennas and Propagation Conference Best Paper Award, in 2007, the Best Poster Award in the field of metamaterial applications in antennas at the Metamaterials Conference, in 2009, the Excellence Award to Young Research Staff at the University Carlos III of Madrid, in 2014, and the Third Place Winner of the Bell Labs Prize, in 2014. She is an Associate Editor of the *IEEE Antennas and Propagation Magazine*, and the IEEE ANTENNAS AND WIRELESS PROPAGATION LETTERS.

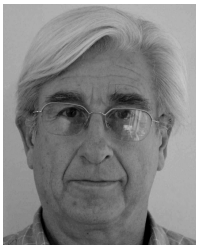

**RODOLFO FEICK** (S'71–M'76–SM'95) received the Ingeniero Civil Electrónico degree from the Universidad Técnica Federico Santa María, Valparaíso, Chile, in 1970, and the Ph.D. degree in electrical engineering from the University of Pittsburgh, Pittsburgh, PA, USA, in 1975. Since 1975, he has been with the Department of Electronics Engineering, Universidad Técnica Federico Santa María, where he is currently an Associate Researcher. His current interests include RF channel modeling, digital communications, microwave system design, and RF measurement.

**REINALDO A. VALENZUELA** (M'85–SM'89–F'99) received the B.Sc. degree from the University of Chile, Santiago, Chile, and the Ph.D. degree from the Imperial College of Science and Technology, University of London, London, U.K. At Bell Laboratories, he studied indoor microwave propagation and modeling, packet reservation multiple access for wireless systems, and optical WDM networks. He became the Manager of the Voice Research Department, Motorola Codex, where he was involved in the implementation integrated voice and data packet systems. On returning to Bell Laboratories, he led a multidisciplinary team to create a software tool for Wireless System Engineering, now in widespread use in Lucent Technologies. His research interests include microwave propagation measurements and models, intelligent antennas, third generation wireless systems, and space-time systems achieving high capacities using transmit and receive antenna arrays. He has published over 80 papers and has 12 patents. He received the Distinguished Member of the Technical Staff Award, and is the Director of the Wireless Communications Research Department. He is an Editor of the IEEE TRANSACTIONS ON COMMUNICATIONS and the IEEE TRANSACTIONS ON WIRELESS COMMUNICATIONS.